

Reaction Mechanisms | Hot Paper |

Dissociative Ionization and Thermal Decomposition of Cyclopentanone

Johan I. M. Pastoors,^[a] Andras Bodi,^[b] Patrick Hemberger,^[b] and Jordy Bouwman^{*[a, c]}

Abstract: Despite the growing use of renewable and sustainable biofuels in transportation, their combustion chemistry is poorly understood, limiting our efforts to reduce harmful emissions. Here we report on the (dissociative) ionization and the thermal decomposition mechanism of cyclopentanone, studied using imaging photoelectron photoion coincidence spectroscopy. The fragmentation of the ions is dominated by loss of CO, C₂H₄, and C₂H₅, leading to daughter ions at *m/z* 56 and 55. Exploring the C₅H₈O⁺ potential energy surface reveals hydrogen tunneling to play an important role in low-energy decarbonylation and probably also in the ethene-loss processes, yielding 1-butene and methylketene cations, respectively. At higher energies, pathways with-

out a reverse barrier open up to oxopropenyl and cyclopropanone cations by ethyl-radical loss and a second ethene-loss channel, respectively. A statistical Rice–Ramsperger–Kassel–Marcus model is employed to test the viability of this mechanism. The pyrolysis of cyclopentanone is studied at temperatures ranging from about 800 to 1100 K. Closed-shell pyrolysis products, namely 1,3-butadiene, ketene, propyne, allene, and ethene, are identified based on their photoion mass-selected threshold photoelectron spectrum. Furthermore, reactive radical species such as allyl, propargyl, and methyl are found. A reaction mechanism is derived incorporating both stable and reactive species, which were not predicted in prior computational studies.

Introduction

In general, biofuels are renewable and often sustainable alternatives to fossil fuels, which can also mitigate harmful emissions.^[1] In particular, more and more research focuses on fuels derived from waste biomass. While fossil fuels are typically composed of mostly carbon and hydrogen, biofuels also contain oxygen in the form of hydroxyl (e.g., ethanol), carboxyl, aldehyde, or ketone functional groups.^[2] Their varying composition leads to differing combustion chemistry, which needs to be thoroughly understood.

One of numerous possible classes of biofuel molecules are ketones. Cyclopentanone is a cyclic ketone of C₅H₈O composi-

tion that can be produced from furfural,^[3,4] which in turn is produced industrially by acidic hydrolysis of hemicellulose, a major constituent of plant matter,^[5] or, alternatively, through pyrolysis of biomass.^[6] Cyclopentanone also serves as a precursor for other, high-density, fuels,^[7] which are suitable for use in airplanes. A thorough understanding of the unimolecular dissociation of cyclopentanone is crucial to accurately model its combustion.

The pyrolysis of cyclic ketones has been studied in some detail. Employing fractional product condensation and IR spectroscopic analysis, Johnson and Walters^[8] found 2-cyclopenten-1-one, 1-butene, ethene, carbon monoxide, and hydrogen as cyclopentanone pyrolysis products. Delles et al.^[9] performed similar experiments and reported the formation of 4-pentenal in addition to products reported by Johnson and Walters.^[8] Several low-molecular-weight species were observed in a gas chromatogram of the reaction mixture, but could not be assigned. Porterfield et al.^[10] studied the pyrolysis of another cycloketone, cyclohexanone (C₆H₁₀O), using flash pyrolysis in combination with photoionization mass spectrometry and matrix isolation Fourier transform infrared (FTIR) spectroscopy. They reported that methylvinyl ketone and ethene are formed through keto–enol tautomerization followed by a retro-Diels–Alder reaction. Furthermore, they argued that the other detected products, among which ketene (C₂H₂O), are formed by means of α , β , or γ C–C bond cleavage followed by rearrangements of the thus formed diradicals.

Cyclopentanone pyrolysis has also been addressed computationally. Zaras et al.^[11] characterized the energetics of the unimolecular dissociation of cyclopentanone using the composite

[a] J. I. M. Pastoors, Dr. J. Bouwman
Radboud University, Institute for Molecules and Materials
FELIX Laboratory, Toernooiveld 7c, 6525 ED Nijmegen (The Netherlands)
E-mail: bouwman@strw.leidenuniv.nl

[b] Dr. A. Bodi, Dr. P. Hemberger
Laboratory for Synchrotron Radiation and Femtochemistry
Paul Scherrer Institute, 5232 Villigen (Switzerland)

[c] Dr. J. Bouwman
Present address: Sackler Laboratory for Astrophysics
Leiden Observatory, Leiden University, P.O. Box 9513
2300 RA Leiden (The Netherlands)

Supporting information and the ORCID identification numbers for the authors of this article can be found under <https://doi.org/10.1002/chem.201702376>.

© 2017 The Authors. Published by Wiley-VCH Verlag GmbH & Co. KGaA. This is an open access article under the terms of Creative Commons Attribution NonCommercial License, which permits use, distribution and reproduction in any medium, provided the original work is properly cited and is not used for commercial purposes.

G3B3 method. They considered C–C scission reactions, among other possible channels, and only found products formed from reactions initiated by α -cleavage, despite the fact that β -cleavage was determined to be lower in energy. The computational results on the neutral cyclopentanone potential energy surface (PES) were employed to calculate rate constants of the initial isomerization steps over the 800–2000 K temperature range by using Rice–Ramsperger–Kassel–Marcus (RRKM) modeling. They concluded that the main products are $C_2H_4 + CO$ and the rate constants suggest that keto–enol isomerization plays a pivotal role in the formation of other products, namely cyclopentanone, 1,3-butadiene, and acetylene.

Wang et al.^[12] performed a combined theoretical and experimental study on the dissociative photoionization of cyclopentanone, providing a detailed $C_5H_8O^+$ PES. Experiments were performed using a femtosecond laser to induce dissociative ionization and time-of-flight (TOF) mass spectrometry for detection of fragments. Based on quantum chemical computations, rates and branching fractions were derived by RRKM modeling.

Literature data to validate the theoretical computations on cyclopentanone dissociation are scarce. In prior experimental pyrolysis studies, product species were assigned offline after condensation, introducing the possibility of secondary reactions and inherently imposing uncertainties on the actual underlying formation mechanism of the detected products. Moreover, these studies were not sensitive to reactive intermediates, which could provide important clues to the overall chemistry. Furthermore, single-photon dissociative ionization data employing parent-ion internal energy selection are not available. However, such data can be used to quantify bond dissociation energies on the cationic surface accurately, and provide details on the underlying dissociation mechanism,^[13] relevant for understanding and modeling, for example, mass spectra.^[14]

Here we report on an experimental study of the (dissociative) ionization and pyrolysis of cyclopentanone, using threshold photoelectron photoion coincidence spectroscopy (TPEPICO).^[15] The pyrolysis products are sampled directly from the pyrolysis reactor and are identified by comparing their threshold photoelectron spectra to data available from the literature. A pyrolysis mechanism is proposed and discussed in light of the recent findings on cyclohexanone pyrolysis. The experimental findings on the dissociative ionization are rationalized by hydrogen tunneling and a model is constructed to test the viability of this fragmentation mechanism.

Results

The ionization, dissociative ionization, and pyrolysis of cyclopentanone have been studied and the results are presented in the next sections. A reaction mechanism is proposed for the dissociative ionization and experimental results on pyrolysis are compared to a computational study from the literature. Supplementary pyrolysis reaction mechanisms are proposed to explain some of the observed products.

Threshold photoelectron spectrum

The cyclopentanone cation has C_2 symmetry and the highest occupied molecular orbital (HOMO), shown together with the mass-selected threshold photoelectron spectrum in Figure 1,

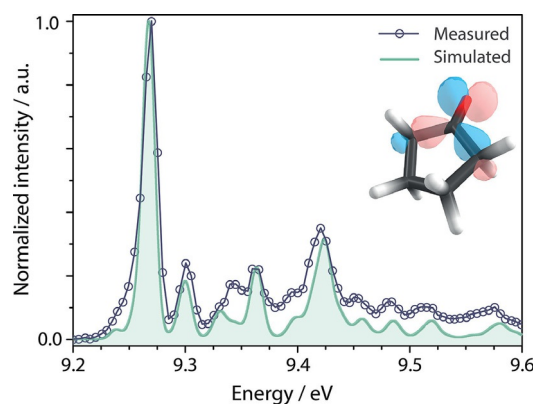


Figure 1. Threshold photoelectron spectrum of cyclopentanone (connected blue circles) displayed together with a Franck–Condon simulation of the spectrum (green). The inset shows the highest occupied molecular orbital on cyclopentanone.

has antibonding character along the C=O bond and bonding character along the two (O=C)–C bonds. Upon ionization through the $\tilde{X}^+ \ ^2B \leftarrow \tilde{X}^1A$ transition, electron density is removed from the HOMO, leading to a 0.02 Å contraction of the C=O bond and a 0.03 Å elongation of the two (O=C)–C bonds, as predicted by B3LYP/6–311 + G(d,p) geometry optimization of the neutral and ionic ground state. The measured spectrum reveals a strong resonance at (9.27 ± 0.02) eV, which is in agreement with the ionization potential for cyclopentanone of (9.25 ± 0.02) eV reported by Chadwick et al.^[16] The simulated spectrum matches the resonances in the measured spectrum very well. Three major features at 9.30, 9.36 and 9.43 eV can be assigned to a CH_2 rocking motion (260 cm^{-1}), a C–C(=O)–C stretching vibration (776 cm^{-1}) and a combination of C=O and a C–C(=O)–C stretch (1268 cm^{-1}).

Dissociative ionization

The dissociative photoionization of cyclopentanone has been studied to distinguish dissociative ionization products from thermal decomposition products.^[17] Furthermore, it is interesting to compare and contrast the fragmentation processes in the neutral molecule, induced by heat in the microreactor, and in the ion, brought about by the excess energy of an ionizing vacuum ultraviolet (VUV) photon. In the breakdown diagram in Figure 2A, the fractional abundance of parent and fragment ions detected in threshold photoionization of the room-temperature sample is plotted as a function of photon energy. The lowest energy channel sets in at around 10.4 eV in the room-temperature sample, and involves the loss of 28 amu, that is, CO or C_2H_4 . The CBS-QB3 calculated dissociative photoionization energies to form the most stable fragment ions, the 1-butene and methylketene cations, are 10.46 and 10.76 eV, re-

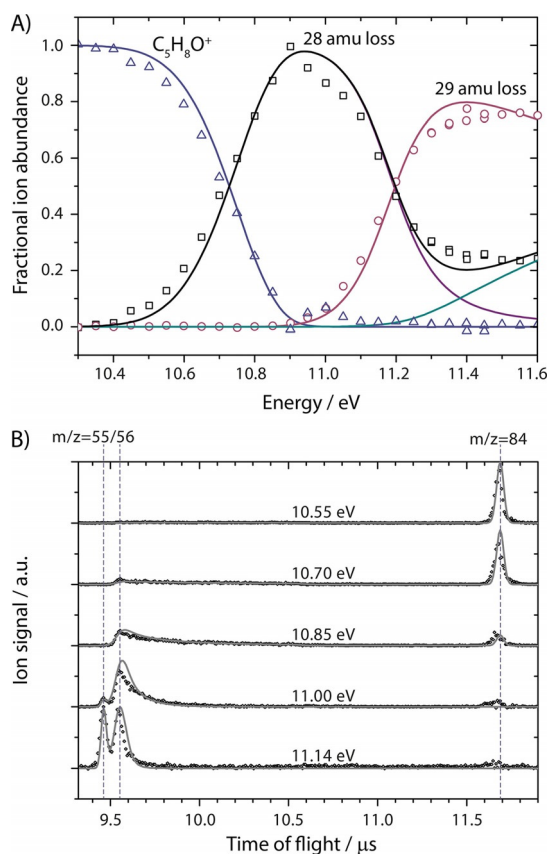


Figure 2. A) The cyclopentanone breakdown diagram showing threshold photoionization fractional parent and daughter ion abundances as a function of photon energy. Open symbols represent experimentally measured values and continuous lines correspond to the RRKM model result. Loss of both CO and C₂H₄ may contribute to the 28 amu product loss at high photon energies, and the individual model contributions are shown (purple and green) together with their sum (black). B) Illustrative threshold photoionization TOF distributions between 10.55 and 11.14 eV. Dots correspond to experimental data, continuous lines represent the statistical model fits.

spectively. As will be discussed later, the formation of the cyclopropanone cation is already possible at its thermochemical onset at 11.26 eV over a loose transition state, but its contribution can be ruled out at low photon energies. On the other hand, loss of 29 amu corresponds unequivocally to the loss of C₂H₅, of which the thermochemical threshold lies at 11.14 eV, more than 0.5 eV lower than HCO loss (11.69 eV).

We note in passing that, upon ionization, the calculated OC-CH₂-CH₂ bond angle increases from 57.6° to 106.3° in cyclopropanone, that is, the cationic minimum is severely distorted. The cyclic structure corresponds to a transition state, which connects the two structures with the carbonyl group coordinated to the each of the CH₂ groups. For sake of simplicity, we continue calling this ion the cyclopropanone cation.

The time-of-flight distributions, shown in Figure 2B, shed light on the competition between the 28 and 29 amu loss channels. The *m/z* 56 peak exhibits a quasi-exponential decay to higher TOF, which is indicative of fragmentation in the acceleration region of the mass spectrometer, and—in the experimental configuration used in this work—a unimolecular rate constant of 10⁴–10⁷ s⁻¹. In contrast, the 29 amu loss peak at

m/z 55 is quite symmetric, suggesting absence of a kinetic shift. Therefore, the rate-determining step in the CO- or C₂H₄-loss channel appears to be a tight transition state, and loss of C₂H₅, associated with a looser transition state, quickly outcompetes 28 amu loss once it is energetically allowed.

The potential energy surface of the C₅H₈O cation is explored considering these insights, and dissociation pathways are proposed in Figure 3. Dissociation is preceded by α-bond breaking

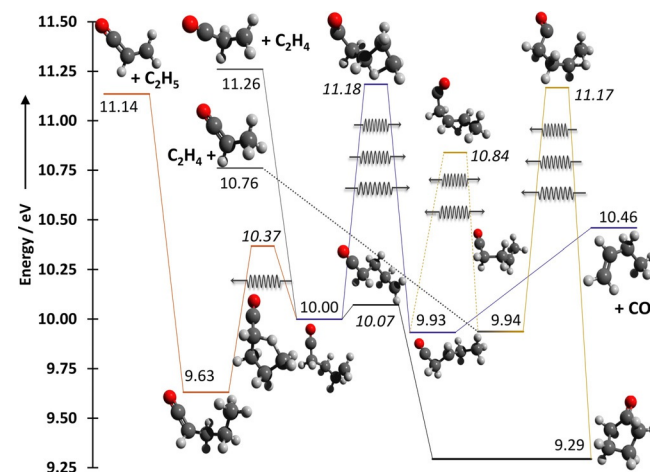


Figure 3. Potential energy diagram displaying transition states and minima in the dissociative photoionization of cyclopentanone. Energy levels obtained using the CBS-QB3 method are shown relative to the neutral and are italicized for transition states. Wavy arrows indicate tunneling contributions in hydrogen-transfer isomerization steps. The dotted line in methylketene formation represents several omitted transition states with increasing energy but all below the energy of the products.

in the parent ion, yielding a straight-chain intermediate at 10.00 eV, which plays a central role in all three fragmentation processes, that is, the loss of C₂H₅, C₂H₄, and CO. Ethene loss to form the cyclopropanone cation comprises the highest energy product channel, but can take place without an energy maximum, along an attractive reaction energy curve. 2,5-Hydrogen transfer results in a slightly more stable isomer over a moderate barrier at 10.37 eV, which may be subject to tunneling, after which an ethyl radical may be expelled. The most stable dissociation products, the 1-butene cation and carbon monoxide, are only accessible after surmounting an energetic 3,5-hydrogen-transfer transition state at 11.18 eV. However, these hydrogen-transfer processes may be enhanced by tunneling, similar to the less dominant methane-loss process in acetone,^[18] which could also explain the low and slowly rising rate constant associated with 28 amu loss. The first, α-bond breaking step in the parent ion may also be accompanied by simultaneous 3,2-hydrogen-atom transfer over a transition state (11.17 eV) that is virtually isoenergetic with the 3,5-hydrogen-transfer transition state mentioned earlier. Although a further, lower energy hydrogen-transfer step may yield the CO-loss precursor isomer at a barrier of 10.84 eV, this step is unlikely to compete with the loss of ethene, yielding the methylketene cation already at 10.76 eV. This process involves CO-transfer and C₂H₄-rotation transition states at progressively higher barriers (omitted in Figure 3, see dotted line), but none is higher in

energy than the products. It is likely that the pure hydrogen-transfer transition state leading to loss of CO is more enhanced by tunneling than the simultaneous opening of the carbon ring and vicinal hydrogen transfer, therefore the product formed from loss of 28 amu is probably mostly the 1-butene cation, but methylketene contributions by loss of ethene cannot be ruled out at energies exceeding 10.76 eV.

In addition to the 28 and 29 amu loss fragment ions, the center-of-gravity analysis^[19] of the parent ion peak revealed trace amounts of hydrogen-loss fragments at around 10.8 eV photon energy. This is much lower than the direct C–H bond breaking dissociative photoionization energy (11.42 eV), which implies isomerization to the enolic parent ion, which subsequently may lose a hydrogen atom already at 10.32 eV, making this the lowest energy dissociative photoionization process discussed herein. The reason for its almost negligible abundance lies in the enolization transition state, which, at 11.54 eV, is also the highest energy structure that appears to play a role in the studied energy range. Similar to the low-energy CO and C₂H₄ losses, enol formation followed by hydrogen loss may take place predominantly by tunneling, and the small hydrogen-loss abundance confirms negligible enol formation in dissociative photoionization.

The dissociative photoionization mechanism shown in Figure 3 is put to the test by constructing a statistical RRKM model based on the computed energetics, assuming that the rate-determining step is the formation of the products for the C₂H₅⁺ and C₂H₄-loss channels, the latter yielding the cyclopropanone cation, and passing over or through the hydrogen-transfer transition state for the CO-loss channel. Since the CO-loss and the low-energy C₂H₄-loss channel are expected to behave rather similarly with the former being the more dominant one, we have not explicitly considered the latter in the model. The hydrogen-atom tunneling rate constants in CO loss were calculated using an Eckart barrier,^[20] and only the transition state transitional mode frequencies were fitted in the high-energy C₂H₄ and C₂H₅ loss, together with the critical tunneling frequency in CO-loss. As shown in Figures 2A and B, the model reproduces the observed ion abundances and dissociation rates quite well, thereby validating the dissociative photoionization mechanism. Only the fitted critical frequency of H tunneling is significantly higher than the calculated one, at 3500 cm⁻¹ vs. 510 cm⁻¹, which suggests a strongly anharmonic barrier and possibly a significant contribution of the low-energy C₂H₄-loss process. The mass spectra also establish the 55 and 56 amu ion signals as the sole dominant low-energy dissociative photoionization products. While the 56 amu signal is also a potential thermal decomposition product of cyclopentanone (*vide infra*), mass-selected threshold photoelectron spectroscopy (ms-TPES) is used to rule out significant 1-butene neutral formation upon pyrolysis. Therefore, dissociative photoionization products do not interfere with the neutral fragments generated through pyrolysis.

Pyrolysis

The pyrolysis of cyclopentanone has been characterized by photoionization mass spectrometry. Pyrolysis products are identified by means of mass-selected threshold photoelectron spectroscopy (ms-TPES) and chemical pathways leading to the detected products are identified.

Mass spectrometry

A typical all-electron time-of-flight mass spectrum of the products and intermediates formed from the pyrolysis of cyclopentanone at about 1100 K and ionized at 10.5 eV is shown in Figure 4. Cyclopentanone is heavily diluted (ca. 0.1%) in argon and species with $m/z \geq 85$ have not been observed, so contributions by bimolecular chemistry are deemed unlikely. The

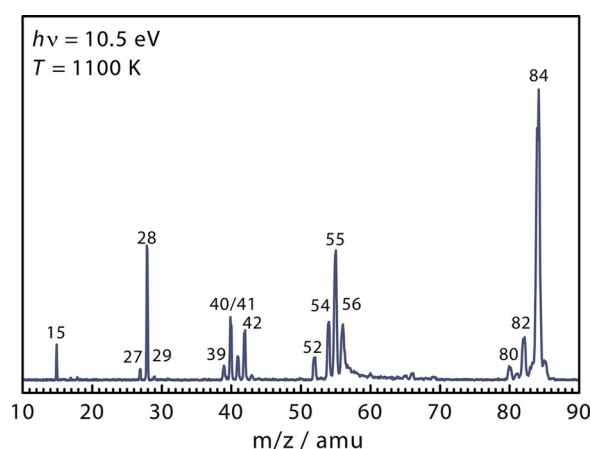


Figure 4. Time-of-flight mass spectrum of cyclopentanone pyrolysis products formed at about 1100 K and ionized at 10.5 eV constructed from coincidences of all photoelectrons regardless of their position on the detector (i.e., energy) with photoions.

peaks at 55 and 56 amu are attributed to dissociative photoionization of thermally excited cyclopentanone as described in the previous section, while all other products are formed by pyrolysis.

Product identifications

Photoion mass-selected threshold photoelectron spectra were recorded to identify products and intermediates formed upon pyrolysis of cyclopentanone. The ms-TPES of the main products at m/z 84, 54, 42, 41, 40, 39, 28 and 15 are shown in Figure 5. The remaining product signals at m/z 27, 52, 80 and 82 that are apparent in Figure 4 are not intense enough for constructing an ms-TPES with sufficient signal-to-noise, and these products are discussed later in light of the overall chemical mechanism.

The most intense peak in Figure 4 corresponds to the precursor molecule as confirmed by the spectra in Figures 1 and 5. The main discrepancies between the two spectra are caused by the difference in spectral resolution, compounded by the

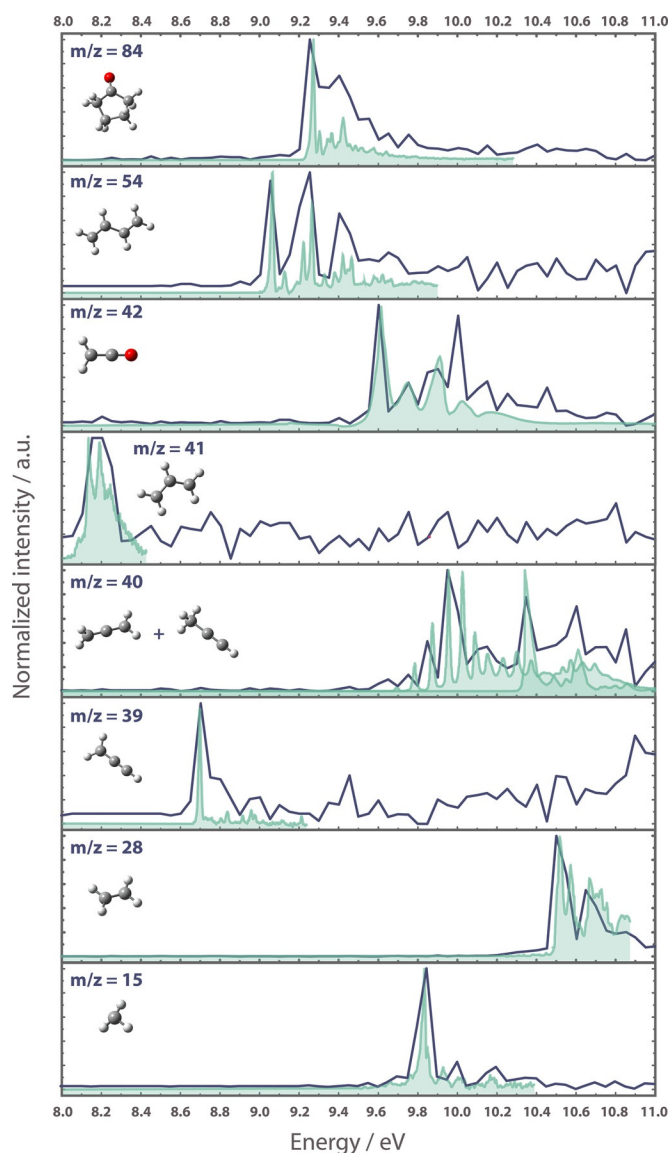


Figure 5. Normalized threshold photoelectron spectra (TPES) of fragments m/z 84, 54, 42, 41, 40, 39, 28, and 15 recorded at 920 K over a photon energy range of 8 to 11 eV in steps of 0.05 eV. Plotted in green are the (threshold) photoelectron spectra of the assigned species taken from the literature.

broadening effect of the higher temperature of the neutrals in the pyrolysis experiment. There is no clear sign of cyclopentenol that may be formed from keto–enol tautomerization and has an ionization threshold at 8.4 eV,^[21] nor is there a clear spectroscopic signature of a linear C_5H_8O isomer that may form upon ring opening.

The pyrolysis product detected at m/z 54 can have a composition of either C_4H_6 or C_3H_2O . The spectrum of 1,3-butadiene^[22]—displayed in green on top of the m/z 54 TPES in Figure 5—matches the measurement very well, leading us to conclude that 1,3-butadiene is the only species contributing to this mass channel. Significant contributions by other species are ruled out based on the absence of spectroscopic signatures (see Supporting Information for more details).^[22–25]

The product detected at m/z 42 can have contributions by isomers of C_3H_6 and C_2H_2O composition. The ms-TPES of this product is compared with photoelectron spectroscopic data of species that may contribute (Supporting Information).^[26–28] The photoelectron spectrum of ketene taken from reference [28] fits our ms-TPES at m/z 42 best (see Figure 5). A small contribution of propene to the overall m/z 42 ms-TPES cannot be ruled out. An additional resonance is observed at around 10 eV, which could be a vibronic band of ketene, but there is a large intensity mismatch. Alternatively, this band could be the result of a vibronic transition of the C_2H_2O tautomer ethynol. In absence of an experimental photoelectron spectrum, the ionization potential is computed at the CBS-QB3 level of theory to be 9.75 eV. No transition is observed around 9.75 eV, rendering contributions from ethynol very unlikely.

The ms-TPES at m/z 41 (Figure 5) exhibits a strong resonance at around 8.2 eV and is in good agreement with the spectrum of the allyl radical.^[29] Cyclopropyl contributions^[30] can be ruled out. Allene, propyne, and cyclopropene can be responsible for the fragment detected at m/z 40. While cyclopropene can be excluded, due to the absence of a resonance at 9.66 eV,^[31] contributions from both allene and propyne are clearly observed, indicating either two different formation channels or a rearrangement between the two isomers. The resonantly stabilized propargyl radical is the only species responsible for the signal observed at m/z 39. The photoelectron spectrum of propargyl is also displayed in Figure 5.^[32,33] Indeed, its photoelectron spectrum resembles that of the product detected here very well. Due to the strong transition at 10.5 eV, the m/z 28 is assigned to ethylene.^[34] Carbon monoxide could contribute to this mass channel as well, but its ionization threshold is 14.01 eV,^[35] beyond the photon energy range of this study. The bottom trace in Figure 5 (m/z 15) is attributed to the methyl radical. The ionization thresholds of the weak signals observed in the mass spectrum (Figure 4) at m/z 52, and m/z 27 correspond to vinylacetylene^[36] and vinyl radicals, respectively.

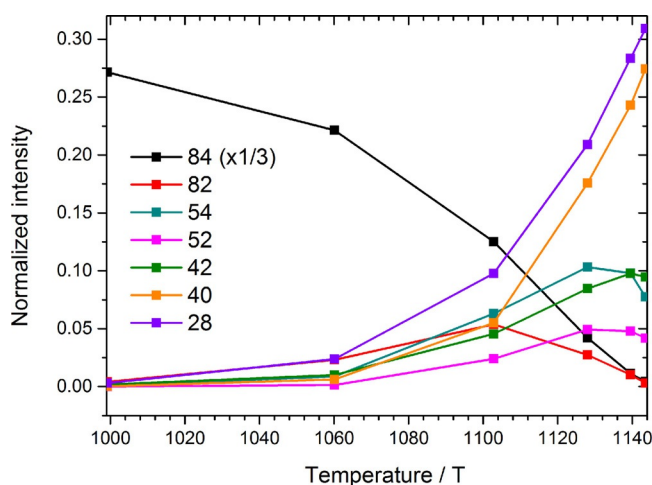


Figure 6. Normalized integrated ion signals as a function of pyrolysis tube temperature for the parent and prominent closed-shell pyrolysis products.

Temperature dependence

Figure 6 shows peak areas as taken from mass spectra at 10.5 eV photon energy as a function of pyrolysis tube temperature. The products at m/z 82 and 28 appear at relatively low temperature, while the other channels open up when the temperature is further increased. Note that the signal strengths may not reflect the absolute abundances, as the intensities are not scaled by absolute ionization cross sections. However, the apparent trend does hold clues to the underlying chemical mechanism.

The ms-TPES data presented in Figure 5 are found to be largely insensitive to the pyrolysis temperature, with the exception of the spectrum taken at m/z 40. This peak is dominated by allene at low temperatures, while a transition/rearrangement to the most stable isomer propyne is observed at higher temperatures (see Supporting Information, Figure S3).

Decomposition mechanism of cyclopentanone

Cyclopentanone pyrolysis products are compared to those predicted in a previous computational study to pin down the underlying dissociation mechanism. A summary of the relevant reaction mechanisms leading to detected species and showing only the rate-limiting transition states as computed by Zaras et al.^[11] is presented in Figure 7.

The fastest chemical reaction according to RRKM calculations is a single-step decomposition leading to CO accompanied by two equivalents of ethene [Eq. (1)].^[11]

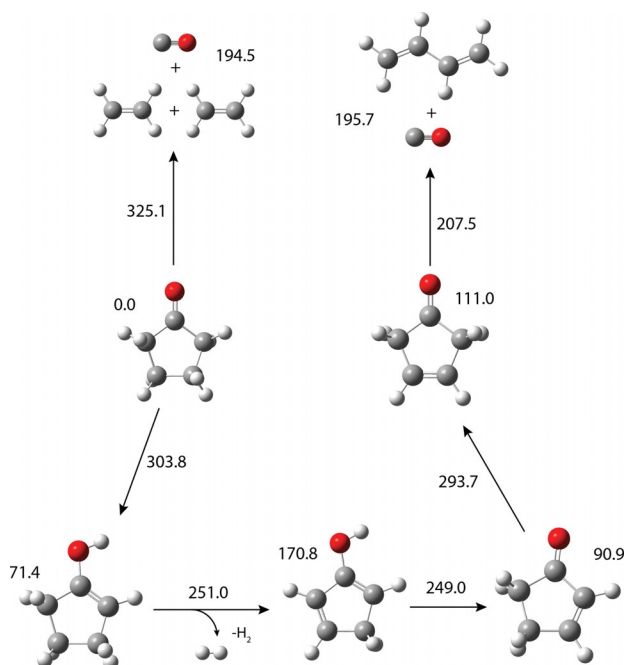


Figure 7. Main low-energy cyclopentanone decomposition pathways reported by Zaras et al.^[11] and confirmed in this work. Arrow labels indicate the energy of the rate-limiting transition state and minimum energies of the pictured structures are also shown in kJ mol^{-1} relative to cyclopentanone.



The barrier involved in this reaction is located at $325.1 \text{ kJ mol}^{-1}$.^[11] Alternatively, α -cleavage of cyclopentanone followed by an isomerization was calculated to result in the same products, albeit at a lower rate. Ethene is confirmed to be one of the main pyrolysis products and its formation sets in at the lowest temperatures (see Figure 6). Carbon monoxide does not ionize in the studied photon energy range, but it is fair to assume that CO is formed as co-product.

The product path to yield 1,3-butadiene and CO was computed to have the lowest overall rate-limiting transition state and proceeds through dehydrogenation to yield 3-cyclopenten-1-one, which subsequently decarbonylates [Eqs. (2) and (3)].^[11]



The dehydrogenation to yield 3-cyclopenten-1-one may proceed directly from cyclopentanone through loss of H_2 , but the multi-step process involving keto-enol tautomerization to 1-cyclopenten-1-ol shown in Figure 7 has a lower rate-limiting barrier. The tautomerization comprises the rate limiting step of $303.8 \text{ kJ mol}^{-1}$. Next, molecular hydrogen is lost to form 1,4-cyclopentadien-1-ol. A subsequent rearrangement via 2-cyclopenten-1-one produces 3-cyclopenten-1-one, from which CO can be eliminated to form 1,3-butadiene. Indeed a signal is observed at m/z 82 and could point to the stabilization of a fraction of the formed $c\text{-C}_5\text{H}_6\text{O}$ species. This signal grows in together with ethene (See Figure 6), but gets depleted quickly as the 1,3-butadiene signal gains in intensity, confirming this reaction pathway. Further dehydrogenation of 2-cyclopenten-1-one may yield 2,4-cyclopentadien-1-one.

In this study, ketene, allene, and propyne as well as the radicals allyl, propargyl, vinyl and methyl have also been identified. However, their formation has neither been predicted computationally previously, nor were these species detected experimentally before.^[9,11] Ketene and allene may be formed from diradicals that form through the α -, β -, or γ -cleavage of cyclopentanone as shown in Figure 8, analogous to the unimolecular decomposition of cyclohexanone.^[10] Both α - and β -cleavage may yield ketene. The accompanying $\cdot\text{CH}_2\text{CH}_2\text{CH}_2\cdot$ diradical further dissociates by means of hydrogen-atom loss to allyl and eventually allene. The detection of allene as a product indicates that ketene, allene, and allyl can be direct decomposition products of cyclopentanone. The mechanism in Figure 8 suggests that α and γ scission may also yield propadienal. However, no clear signature is found in the ms-TPES, suggesting that alternative decomposition processes proceed at a higher rate.

Further unimolecular dissociation and isomerization of products formed from the initial pyrolysis of cyclopentanone also need to be considered as possible contributors to signals observed in the mass spectrum that have not been assigned so far. First, C_3H_3^+ can form through dissociative ionization of allyl

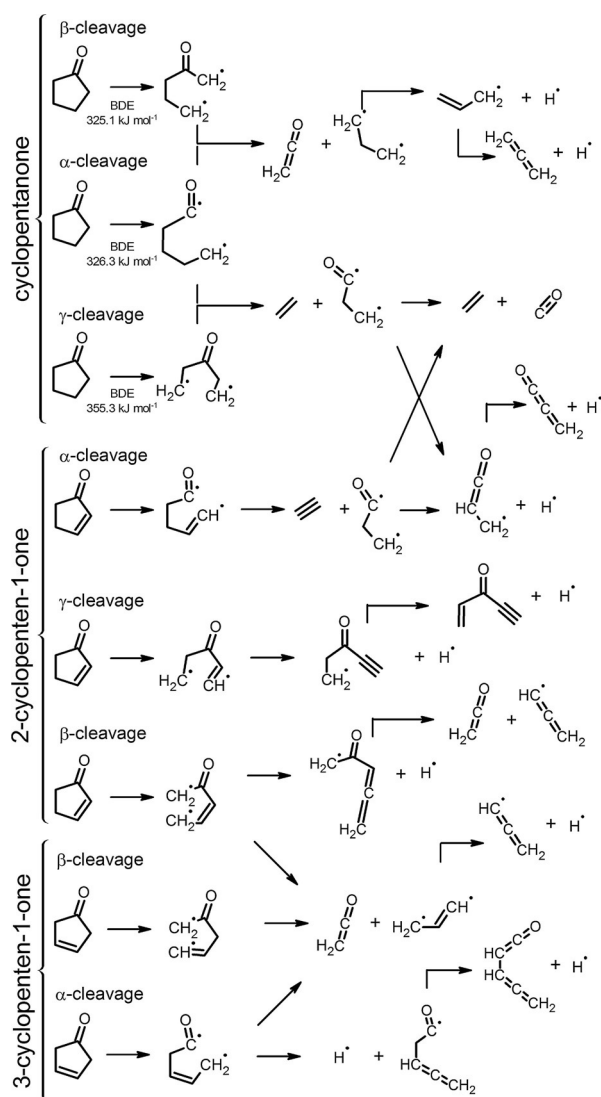
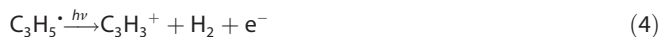


Figure 8. Decomposition pathways of cyclopentanone and cyclopentenone through α -, β -, and γ -cleavage. Computed bond dissociation energies (BDE) are taken from Zaras et al.^[11]

[Eq. (4)] or, alternatively, through thermal dissociation of allyl followed by ionization [Eqs. (5) and (6)].^[17,29]



Another possible channel to allyl proceeds via cyclopentanone. The formation of cyclopentenone + H₂ was computed to be one of the lowest energy pathways for dissociation of cyclopentanone (Figure 7) and its subsequent dissociation through α -, β -, and γ -cleavage is summarized in Figure 8. The detection of propargyl could point to cyclopentenone also being an intermediate species in ketene formation. A TOF mass spectrum recorded at 11.5 eV (i.e., above the ionization poten-

tial of acetylene, see Supporting Information) reveals a signal at m/z 26, confirming that subsequent dissociation of cyclopentenone indeed contributes to the detected products, as no alternative pathway can explain the formation of acetylene.

Pyrolysis of 1,3-butadiene as formed from dissociation of cyclopentanone could also contribute to the detected products. Its pyrolysis has been studied in the past^[37] and was found to proceed mostly by means of the reaction shown in Equation (7).



In the photoionization mass spectra reported by Chambreau et al.,^[37] products are also seen in the mass channels corresponding to vinylacetylene (C₄H₄) and vinyl (C₂H₃). Thus, thermal decomposition of 1,3-butadiene could also explain the formation of these products, although the temperatures reported for the decomposition of butadiene exceed 1000 K and are thus rather high compared to the temperatures used herein. The formation of vinyl and methyl radicals can alternatively proceed by diradical driven disproportionation reactions, which are summarized in the Supporting Information. Atomic hydrogen is abundantly formed according to the proposed cyclopentanone dissociation mechanism and, although the density of the parent molecule in the reactor is kept low (ca. 0.1%), secondary reactions initiated by atomic hydrogen may have a small contribution to the formation of the observed products, or isomerization thereof.

The m/z 40 peak is the only one to exhibit a clearly temperature-dependent isomer composition. Allene is the dominant isomer at low temperatures and is converted to propyne at the highest temperature. The formation of allene is expected from the mechanisms proposed in Figure 8. Isomerization of allene to propyne has been studied extensively in the past and propyne is the most stable isomer.^[38,39] Alternatively, propyne formation can already be initiated in the thermally excited C₅H₈O by the increased hydrogen mobility. These two mechanisms cannot be discerned in the current experiments.

Discussion and Conclusions

The dissociative ionization and pyrolysis of cyclopentanone have been studied on the iPEPICO (imaging photoion photoelectron coincidence) instrument at the VUV beamline of the Swiss Light Source. The dissociative ionization between 10.3 and 11.7 eV yields product ions at m/z 56 and 55 that are formed through loss of CO, C₂H₄ and C₂H₅^{*}. The potential energy surface has been characterized and it is found that the formation of the m/z 56 product proceeds by means of hydrogen tunneling and results in the 1-butene cation and CO and also the methylketene cation plus ethylene for energies exceeding 10.76 eV. The high-energy ethene loss yielding the cyclopropanone cation starts to contribute to this mass channel at energies exceeding 11.26 eV. The m/z 55 product is formed through loss of C₂H₅ with a barrier at 11.14 eV. An RRKM model is employed to support the validity of the proposed hydrogen-tunneling mechanism.

The potential energy surface of the dissociative ionization of C_5H_8O presented here differs slightly from that reported previously.^[12] First, the lowest energy pathway leading to the $C_3H_4O + C_2H_4$ reported by Wang et al.^[12] yields cyclopropanone at an energy of $170.7 \text{ kJ mol}^{-1}$ (1.77 eV) relative to the cation. In this work, we find that this channel is significantly higher (by 0.2 eV) in energy at 1.97 eV with respect to the cation (11.26 eV w.r.t. to the neutral). In addition, the calculations presented here provide an additional pathway to an alternative C_3H_4O product, methylketene. This channel requires 0.5 eV less energy than the cyclopropanone pathway with a rate-limiting barrier located at 11.17 eV and all other barriers below the thermochemical threshold. Moreover, this rate-limiting barrier is subject to tunneling, making this a viable contributor to dissociation for energies exceeding 10.76 eV . Lastly, a noticeable difference lies in the CO-loss channel. In addition to the concerted ring opening and hydrogen shift at a barrier of 11.17 eV reported here and by Wang et al.,^[12] we also located a practically isoenergetic transition state (at 11.18 eV) that involves ring opening followed by migration of a hydrogen (i.e., a non-concerted channel), making it somewhat more likely to dominate the CO-loss mechanism. The detection of a very weak signal at m/z 83 indicates that keto-enol tautomerization only plays a minor role in dissociative photoionization.

Cyclopentanone pyrolysis products formed at a temperature ranging from 800 to 1100 K have been identified by means of ms-TPES of the species sampled directly from the pyrolysis tube reactor. The main identified product species are ethene, 1,3-butadiene, ketene, allene, propyne, allyl, propargyl, and methyl. Vinylacetylene, acetylene, and vinyl radicals have also been observed, but only as trace species. Allene and propyne are found to be the only isobaric products that are sensitive to the reactor temperature, with allene being the dominant C_3H_4 isomer at low and propyne at high temperature.

Previous experimental studies on cyclopentanone pyrolysis identified 2-cyclopenten-1-one, 1-butene, ethene, carbon monoxide, 4-pentenal, and hydrogen as products. Of these species, only C_2H_4 is positively identified and CO and H_2 are likely present, but evade detection at the photon energies used. The non-detection of 1-butene in our experiments can be caused by the fact that it dissociates further at the temperatures applied in our study, or a small fraction of 1-butene could be hidden in the large signal at m/z 56 caused by dissociative ionization. However, close inspection of this signal does not reveal indications of a significant fraction of 1-butene. The non-detection of 1-butene in this study could be due to 1-butene's prompt dissociation by C–C fission [Eq. (8)].



An alternative and more likely explanation is that in the previous pyrolysis experiments 1-butene is formed from bimolecular reactions in the pyrolysis tube, rather than through direct pyrolysis of cyclopentanone. The fact that 1-butene formation has been computed to have a rate-limiting barrier of $462.8 \text{ kJ mol}^{-1}$ and that an RRKM model predicts low formation rate^[11] supports this explanation.

Ketene and allene had not been detected in previous experimental studies, nor had they been predicted from computations. Zaras et al.^[11] did not identify pathways through β -cleavage, although it was established that this is the weakest C–C bond in the molecule. The unambiguous identification of ketene and allene from this study clearly points to the importance of β -cleavage in the pyrolysis of cyclopentanone and a more detailed computational study needs to be undertaken to characterize the energetics and kinetics of this reaction pathway. It is interesting to note that the decomposition in our pyrolytic microreactor and upon dissociative ionization share similar reaction products, such as CO, C_2H_4 and $C_2H_5^{\cdot}$. Thus, understanding the dissociative photoionization mechanism is important, because the onset of dissociative ionization can be shifted towards lower photon energies at elevated temperatures, which may be wrongly assigned to decomposition upon pyrolysis.^[40,41] In addition, similar fragmentation connects both the neutral molecules' and ions' potential energy surface, which can be used to derive heats of formation of reactive intermediates in the absence of a reverse barrier.^[42] It is also interesting to note an important difference between dissociative photoionization process and pyrolysis mechanisms. Keto-enol tautomerization appears to play a crucial role in the formation of butadiene on the neutral PES, while tautomerization is out-competed by other product channels on the ionic surface. However, even on the neutral surface, tautomerization involves a higher barrier than subsequent hydrogen abstraction, which means that the enol only acts as a short-lived intermediate and dissociates promptly.

The findings reported here can also be compared to experimental work reported on cyclohexanone. Porterfield et al.^[10] found that keto-enol tautomerization followed by a retro Diels–Alder fragmentation is responsible for the formation of $CH_2=C(OH)-CH=CH_2 + C_2H_4$. Ring cleavage reactions and subsequent decomposition reactions had been proposed to yield the other observed products, among which species also observed in the pyrolysis of cyclopentanone reported here, such as 1,3-butadiene, ketene and allene, allyl. In contrast with their work, enols have not been detected in our study. Furthermore, analogous to the retro Diels–Alder reaction proposed by Porterfield, a retro [2+2] cycloaddition reaction yielding ketene and allene could occur for cyclopentanone after reorganization to a four-membered ring; however, this processes is energetically unfavorable in cyclopentanone and it is more likely that ketene and allene are formed upon α - or β -ring cleavage reactions instead.

Our results exemplify the power of isomer-resolved product detection in flash pyrolysis using ms-TPES recorded by iPEPICO. Reactive product species, such as ketene and a number of radicals, have been sampled directly from the reactor and have been identified unambiguously. The multiplexed nature of ms-TPES offers a clear advantage over the use of FTIR matrix isolation spectroscopy to assign products; spectral information is obtained mass selectively and isomer specific identification of the products are readily made.^[22] The detection of the first generation of species from the reactor reveals the true under-

lying chemical mechanism and supplies crucial information that is needed for modeling the combustion of biofuels.

Experimental Section

The experiments were performed on the iPEPICO instrument at the vacuum ultraviolet (VUV) beamline of the Swiss Light Source. A short description of the experimental setup is presented here and a more extensive description of the apparatus can be found elsewhere.^[43] Synchrotron VUV radiation produced by a bending magnet was collimated, dispersed in grazing incidence by a grating, and focused at the exit slit in a differentially pumped noble gas filter, which serves to remove higher order radiation. The ionization and detection chamber was flanged onto the exit port of the gas filter, and the photon beam size was about 4×2 mm in the interaction region. Dissociative photoionization measurements were recorded using a $600 \text{ grooves mm}^{-1}$ grating. A grating with $150 \text{ grooves mm}^{-1}$ was used for recording mass-selected threshold photoelectron spectra (ms-TPES) of the pyrolysis products. This grating was selected to enhance the VUV photon flux in the interaction region and, thus, signal levels by an order of magnitude at a reduced photon energy resolution. The photon energy was tuned from 8.0 to 11.7 eV in steps of 0.05 eV for pyrolysis measurements and in steps of 0.025 eV for the dissociative photoionization experiments.

Cyclopentanone (Sigma-Aldrich, >99%) was seeded in argon carrier gas at a concentration of 0.1% and a backing pressure of 1.1 bar. The mixture entered a resistively heated microtubular reactor of about 4 cm in length and 1 mm inner diameter through a $100 \mu\text{m}$ orifice. The temperature on the outer surface of the reactor is monitored by means of a "type C" thermocouple. Based on the extensive simulations by Guan et al.,^[44] the temperature on the centerline of the reactor may be 25% lower than that measured on the outside. The pressure at the entrance of the microreactor was only a few mbar and dropped in the heated zone towards the exit of the tube. The sample expanded into the source chamber, which was maintained at about 1×10^{-4} mbar. The residence time was estimated to be of the order of 10 to $100 \mu\text{s}$.

The gas mixture containing the pyrolysis products exited the reactor tube and was skimmed by a 1 mm diameter skimmer, allowing only the central part of the expansion to reach the ionization volume in the iPEPICO detection chamber, in which the molecular beam intersects the monochromatic ionizing radiation from the VUV beamline. A constant 120 V cm^{-1} electric field accelerated the photoelectrons towards a RoentDek delay line detector, where they were velocity map imaged. The positions of the electrons on the detector contained information on their kinetic energy and their arrival time served as the start signals for the TOF measurements of the cations. Threshold photoelectron spectra were plotted by selecting only the central spot on the electron detector and subtracting the "hot" electron background.^[45] Cations were accelerated in the opposite direction in a Wiley-McLaren type TOF configuration and detected with a microchannel plate (MCP) detector. The mass resolution achieved in the experimental system was $m/\Delta m = 125$.

Coincidences between electrons and cations were plotted as a function of delay time to yield the TOF mass spectra. Those obtained by considering coincidences between all electrons and ions, regardless of the electron energies, are referred to as all-electron mass spectra. Isomer selective product identification is based on ms-TPES, for which only coincidences between threshold electrons (kinetic energy < 10 meV) and ions of a specific time of flight, and

hence mass, were used. Internal energy selection was also achieved by threshold photoionization, because the photon energy minus the adiabatic ionization energy was quantitatively converted to the internal energy of the parent ion. This excess energy and the original thermal energy of the sample was available for fragmentation. When studying dissociative photoionization processes, the threshold ionization fractional parent and daughter ion abundances were plotted in the breakdown diagram, which often contains clues as to the fragmentation mechanism,^[46] and can be modeled quantitatively using statistical thermodynamics approaches to determine accurate dissociative photoionization thresholds.^[47] Furthermore, owing to the long acceleration region and low extraction field, it took several microseconds for the photoions to reach their terminal velocity in the mass spectrometer. If a dissociation process occurs during this time, the fragment ion will have a lower than nominal kinetic energy, and a higher time of flight than promptly formed ions of the same mass. This results in TOF peak profiles that are broadened towards higher TOF, and were modeled to extract unimolecular dissociation rate constants in the $10^4 \text{ s}^{-1} < k(E) < 10^7 \text{ s}^{-1}$ range. The experimental rate curves were also modeled to take kinetic shifts into account.

Computational methods

Quantum chemical calculations using the Gaussian 09^[48] suite of programs were performed to explore the $\text{C}_5\text{H}_8\text{O}^+$ PES to yield insights into the chemical pathways leading to the products formed from dissociative ionization. Reaction coordinates were scanned at the B3LYP/6-311++G(d,p) level of theory to locate transition states and intermediates. Subsequent re-optimizations at the CBS-QB3 level of theory were performed to compute accurate energies. These energies and the B3LYP computed vibrational frequencies were used as input for a statistical model to fit both the breakdown diagram and the time-of-flight profiles using the PEPICO program.^[47]

The B3LYP/6-311++G(d,p) optimized geometries and vibrational normal modes of the electronic ground state of the neutral and cation were used as input for Franck-Condon simulations of the photoionization spectrum. The program ezSpectrum^[49] was employed to compute the spectral intensities of the vibronic transitions and the resulting stick diagram was convoluted with a Gaussian profile with a full-width-at-half-maximum (FWHM) of 100 cm^{-1} to account for the rotational envelope and to facilitate comparison with the experimental data.

Acknowledgements

J.B. acknowledges the Netherlands Organisation for Scientific Research (NWO) for a VENI grant (Grant number 722.013.014). This work was further supported by NWO Exacte Wetenschappen (Physical Sciences) for the use of the supercomputer facilities at SurfSara. A.B. and P.H. acknowledge funding by the Swiss Federal Office for Energy (BFE Contract number SI/501269-01).

Conflict of interest

The authors declare no conflict of interest.

Keywords: flash pyrolysis · high-temperature chemistry · photoelectron spectroscopy · reaction mechanisms · renewable resources

- [1] C. K. Westbrook, *Annu. Rev. Phys. Chem.* **2013**, *64*, 201–219.
- [2] S. K. Hoekman, A. Broch, C. Robbins, E. Cenicerros, M. Natarajan, *Renewable Sustainable Energy Rev.* **2012**, *16*, 143–169.
- [3] M. Hronec, K. Fulajtrova, T. Sotk, *Appl. Catal. B* **2014**, *154–155*, 294–300.
- [4] M. Winfough, K. Voronova, G. Muller, G. Laguisma, B. Sztray, A. Bodi, G. Meloni, *J. Phys. Chem. A* **2017**, *121*, 3401–3410.
- [5] P. McKendry, *Bioresour. Technol.* **2002**, *83*, 37–46.
- [6] A. Demirbas, *Fuel Process. Technol.* **2007**, *88*, 591–597.
- [7] J. Yang, N. Li, G. Li, W. Wang, A. Wang, X. Wang, Y. Cong, T. Zhang, *Chem. Commun.* **2014**, *50*, 2572–2574.
- [8] E. R. Johnson, W. D. Walters, *J. Am. Chem. Soc.* **1954**, *76*, 6266–6271.
- [9] F. M. Delles, L. T. Dodd, L. F. Lowden, F. J. Romano, L. G. Daignaul, *J. Am. Chem. Soc.* **1969**, *91*, 7645–7647.
- [10] J. P. Porterfield, N. Thanh Lam, J. H. Baraban, G. T. Buckingham, T. P. Troy, O. Kostko, M. Ahmed, J. F. Stanton, J. W. Daily, G. B. Ellison, *J. Phys. Chem. A* **2015**, *119*, 12635–12647.
- [11] A. M. Zaras, S. Thion, P. Dagaut, *Int. J. Chem. Kinet.* **2015**, *47*, 439–446.
- [12] Q. Wang, D. Wu, M. Jin, F. Liu, F. Hu, X. Cheng, H. Liu, Z. Hu, D. Ding, H. Mineo, Y. A. Dyakov, A. M. Mebel, S. D. Chao, S. H. Lin, *J. Chem. Phys.* **2008**, *129*, 204302.
- [13] O. Kostko, B. Bandyopadhyay, M. Ahmed, *Annu. Rev. Phys. Chem.* **2016**, *67*, 19–40.
- [14] C. A. Bauer, S. Grimme, *J. Phys. Chem. A* **2016**, *120*, 3755–3766.
- [15] T. Baer, R. P. Tuckett, *Phys. Chem. Chem. Phys.* **2017**, *19*, 9698–9723.
- [16] L. Weiler, D. Chadwick, D. C. Frost, *J. Am. Chem. Soc.* **1971**, *93*, 4320–4321.
- [17] J. Bouwman, A. Bodi, J. Oomens, P. Hemberger, *Phys. Chem. Chem. Phys.* **2015**, *17*, 20508–20514.
- [18] A. Bodi, T. Baer, N. K. Wells, D. Fakhoury, D. Klecyngier, J. P. Kercher, *Phys. Chem. Chem. Phys.* **2015**, *17*, 28505–28509.
- [19] B. West, C. Joblin, V. Blanchet, A. Bodi, B. Sztaray, P. M. Mayer, *J. Phys. Chem. A* **2012**, *116*, 10999–11007.
- [20] A. Bodi, B. Sztaray, T. Baer, *Phys. Chem. Chem. Phys.* **2006**, *8*, 613–623.
- [21] G. Meloni, T. M. Selby, D. L. Osborn, C. A. Taatjes, *J. Phys. Chem. A* **2008**, *112*, 13444–13451.
- [22] A. Bodi, P. Hemberger, D. L. Osborn, B. Sztaray, *J. Phys. Chem. Lett.* **2013**, *4*, 2948–2952.
- [23] K. B. Wiberg, G. B. Ellison, J. J. Wendoloski, C. R. Brundle, N. A. Kuebler, *J. Am. Chem. Soc.* **1976**, *98*, 7179–7182.
- [24] J. D. Savee, S. Borkar, O. Welz, B. Sztaray, C. A. Taatjes, D. L. Osborn, *J. Phys. Chem. A* **2015**, *119*, 7388–7403.
- [25] W. Harshbarger, N. A. Kuebler, M. B. Robin, *J. Chem. Phys.* **1974**, *60*, 345–350.
- [26] A. Katrib, J. W. Rabalais, *J. Phys. Chem.* **1973**, *77*, 2358–2363.
- [27] P. Rademacher, *Chem. Rev.* **2003**, *103*, 933–975.
- [28] C. Baker, D. W. Turner, *J. Chem. Soc. D* **1969**, 480–481.
- [29] I. Fischer, T. Schler, H.-J. Deyerl, M. Elhanine, C. Alcaraz, *Int. J. Mass Spectrom.* **2007**, *261*, 227–233.
- [30] J. Dyke, A. Ellis, N. Jonathan, A. Morris, *J. Chem. Soc. Faraday Trans. 2* **1985**, *81*, 1573–1586.
- [31] K. Vasilatou, J. M. Michaud, D. Baykusheva, G. Grassi, F. Merkt, *J. Chem. Phys.* **2014**, *141*, 064317.
- [32] H. Gao, Z. Lu, L. Yang, J. G. Zhou, C. Y. Ng, *J. Chem. Phys.* **2012**, *137*, 161101.
- [33] P. Hemberger, M. Lang, B. Noller, I. Fischer, C. Alcaraz, B. K. C. de Miranda, G. A. Garcia, H. Soldi-Lose, *J. Phys. Chem. A* **2011**, *115*, 2225–2230.
- [34] R. Stockbauer, M. G. Inghram, *J. Electron Spectrosc. Relat. Phenom.* **1975**, *7*, 492–496.
- [35] P. Erman, A. Karawajczyk, E. Rachlewskallne, C. Stromholm, J. Larsson, A. Persson, R. Zerne, *Chem. Phys. Lett.* **1993**, *215*, 173–178.
- [36] T. A. Cool, J. Wang, K. Nakajima, C. A. Taatjes, A. McIlroy, *Int. J. Mass Spectrom.* **2005**, *247*, 18–27.
- [37] S. D. Chambreau, J. Lemieux, L. Wang, J. Zhang, *J. Phys. Chem. A* **2005**, *109*, 2190–2196.
- [38] A. Lifshitz, M. Frenklach, A. Burcat, *J. Phys. Chem.* **1976**, *80*, 2437–2443.
- [39] M. Yoshimine, J. Pacansky, N. Honjou, *J. Am. Chem. Soc.* **1989**, *111*, 4198–4209.
- [40] S. Liang, P. Hemberger, N. M. Neisius, A. Bodi, H. Grützmacher, J. Levalois-Grützmacher, S. Gaan, *Chem. Eur. J.* **2015**, *21*, 1073–1080.
- [41] S. Liang, P. Hemberger, J. Levalois-Grützmacher, H. Grützmacher, S. Gaan, *Chem. Eur. J.* **2017**, *23*, 5595–5601.
- [42] F. Holzmeier, I. Wagner, I. Fischer, A. Bodi, P. Hemberger, *J. Phys. Chem. A* **2016**, *120*, 4702–4710.
- [43] A. Bodi, M. Johnson, T. Gerber, Z. Gengeliczki, B. Sztaray, T. Baer, *Rev. Sci. Instrum.* **2009**, *80*, 034101.
- [44] Q. Guan, K. N. Urness, T. K. Ormond, D. E. David, G. B. Ellison, J. W. Daily, *Int. Rev. Phys. Chem.* **2014**, *33*, 447–487.
- [45] B. Sztaray, T. Baer, *Rev. Sci. Instrum.* **2003**, *74*, 3763–3768.
- [46] P. Hemberger, A. Bodi, T. Gerber, M. Wuertemberger, U. Radius, *Chem. Eur. J.* **2013**, *19*, 7090–7099.
- [47] B. Sztaray, A. Bodi, T. Baer, *J. Mass Spectrom.* **2010**, *45*, 1233–1245.
- [48] Gaussian 09, Revision D.01, M. J. Frisch, G. W. Trucks, H. B. Schlegel, G. E. Scuseria, M. A. Robb, J. R. Cheeseman, G. Scalmani, V. Barone, B. Menonucci, G. A. Petersson, H. Nakatsuji, M. Caricato, X. Li, H. P. Hratchian, A. F. Izmaylov, J. Bloino, G. Zheng, J. L. Sonnenberg, M. Hada, M. Ehara, K. Toyota, R. Fukuda, J. Hasegawa, M. Ishida, T. Nakajima, Y. Honda, O. Kitao, H. Nakai, T. Vreven, J. A. Montgomery, Jr., J. E. Peralta, F. Ogliaro, M. Bearpark, J. J. Heyd, E. Brothers, K. N. Kudin, V. N. Staroverov, T. Keith, R. Kobayashi, J. Normand, K. Raghavachari, A. Rendell, J. C. Burant, S. S. Iyengar, J. Tomasi, M. Cossi, N. Rega, J. M. Millam, M. Klene, J. E. Knox, J. B. Cross, V. Bakken, C. Adamo, J. Jaramillo, R. Gomperts, R. E. Stratmann, O. Yazyev, A. J. Austin, R. Cammi, C. Pomelli, J. W. Ochterski, R. L. Martin, K. Morokuma, V. G. Zakrzewski, G. A. Voth, P. Salvador, J. J. Dannenberg, S. Dapprich, A. D. Daniels, O. Farkas, J. B. Foresman, J. V. Ortiz, J. Cioslowski, D. J. Fox, Gaussian, Inc., Wallingford CT, **2013**.
- [49] V. Mozhaykiy, A. I. Krylov, ezSpectrum: <http://iopenshell.usc.edu/downloads>.

Manuscript received: May 24, 2017

Accepted manuscript online: July 10, 2017

Version of record online: August 31, 2017